

Flux tube profiles at finite temperature

Sodbileg Chagdaa* and Edwin Laermann

Faculty of Physics, University of Bielefeld, D-33501 Bielefeld, Germany

E-mail: sodbileg@physik.uni-bielefeld.de

We present finite temperature results of profiles of a flux tube connecting a static $q\bar{q}$ pair. In particular, we study the behavior of the flux tube in the vicinity of the phase transition temperature. The simulations have been carried out in $SU(2)$ gauge theory at two values of N_τ on lattices with volumes 8^3 , 16×8^2 and 24×12^2 . A detailed investigation of the longitudinal and transverse distribution of energy and action is presented. It has been found that the physical width of the flux tube D_ε decreases strongly with temperature T , while the width of the action density increases.

*The XXV International Symposium on Lattice Field Theory
July 30 - August 4 2007
Regensburg, Germany*

*Speaker.

1. Introduction

One of the most striking physical properties of QCD is confinement of quarks in a hadron so that only colour singlets can be produced and observed. The searches for free quark particles have been proven to be unsuccessful basically because of the attractive potential, which rises linearly with the quark-antiquark separation. The linearly confining potential in QCD is due to the presence of flux tubes. In the flux tube picture, the chromoelectric field originating from a quark does not spread uniformly in space, but is squeezed into tubes of constant cross section. As two quarks separate, the gluon fields form narrow tubes of colour charge. QCD lattice simulations predict that above a certain temperature (T) or density, nuclear matter could undergo a phase transition after which quarks and gluons are deconfined from hadrons, and form a new state of matter called quark-gluon plasma (QGP). Investigating the behaviour of matter in the vicinity of the transition is a major goal of current and planned experiments with heavy ion collisions. Motivated by the flux tube distributions at zero temperature [2, 3, 4, 5], interesting questions arise at finite or high temperature, concerning the behaviour of the flux tube when QCD undergoes a phase transition. There is numerical evidence that the slope of the linearly rising inter-quark potential decreases as temperature increases [1]. This means that the string tension is no longer constant but is T -dependent and becomes smaller close to T_c . Above T_c , the static potential is expected to be exponentially screened. This leads to the following questions: What steps will the flux tube pass through and how does it behave when it undergoes a phase transition? What are the T -dependence of the width and maximum value of the energy density of the flux tube? We tried to have answers to these questions in this paper.

2. Flux tube model

In the flux tube model, the gluon fields form tubes connecting two quarks. One can look into the details of the interaction between quark pairs studying the distribution of the chromoelectric and chromomagnetic components of these fields which compose energy and action density of the flux tube. To obtain the flux data at finite T one has to choose the temporal size of the lattice to be short so that the physical T is large. The T and volume can be expressed in terms of the lattice spacing a , which is a function of the coupling constant β , thus we can vary T by changing the coupling constant. The distribution of gluon fields in the flux tube is measured as follows. Time propagation of the two static quarks sitting in the ends of the flux tube are represented by Polyakov loop L and its conjugate L^+ , which are located at distance r from each other on the lattice, where Polyakov loop, $L(\mathbf{r}) \equiv \frac{1}{N_c} Tr \prod_{\tau=1}^{N_\tau} U_4(\mathbf{r}, \tau)$, consists of a product of link variables along closed curves, which wind around the torus in temporal direction. The plaquette variable $\square_{\mu\nu} = \frac{1}{N_c} Tr(U_{\mu,\nu})$ with the orientation (μ, ν) , which has six different values (2,3), (1,3), (1,2), (1,4), (2,4), (3,4), measures the field strength. Thus, the central observables that govern the event in the flux tube can be extracted from the correlation of a plaquette with the Polyakov loops

$$f_{\mu\nu}(\mathbf{r}, \mathbf{x}) = \frac{\beta}{a^4} \left[\frac{\langle L(0)L^+(\mathbf{r})\square_{\mu\nu}(\mathbf{x}) \rangle}{\langle L(0)L^+(\mathbf{r}) \rangle} - \langle \square_{\mu\nu} \rangle \right]. \quad (2.1)$$

\mathbf{x} denotes the distance of the plaquette from the line connecting quark sources and \mathbf{r} is the quark separation. The flux tube profiles can be probed by varying the distance and the orientation of

the plaquette with respect to the Polyakov loop, over 3-space (x, y, z) . The six different (μ, ν) combinations define the six components of electric and magnetic fields. The three space-space plaquettes correspond to the magnetic fields and three space-time plaquettes correspond to the electric fields:

$$f_{23} \rightarrow \frac{1}{2}(-B_{\perp}^2) \quad (2.2) \quad f_{14} \rightarrow \frac{1}{2}E_{\perp}^2 \quad (2.5)$$

$$f_{13} \rightarrow \frac{1}{2}(-B_{\perp}^2) \quad (2.3) \quad f_{24} \rightarrow \frac{1}{2}E_{\perp}^2 \quad (2.6)$$

$$f_{12} \rightarrow \frac{1}{2}(-B_{\parallel}^2) \quad (2.4) \quad f_{34} \rightarrow \frac{1}{2}E_{\parallel}^2. \quad (2.7)$$

The directions of orientations of the field components (i.e orthogonal and parallel) describe their orientation to the axis connecting $q\bar{q}$. The total energy and action density are

$$\varepsilon = \frac{1}{2}(E^2 + B^2) \quad (2.8)$$

$$\delta = \frac{1}{2}(E^2 - B^2) \quad (2.9)$$

where E and B are the sum of the three electric and three magnetic components, respectively.

2.1 Details of the simulation

By means of Monte Carlo we simulated pure gauge theory with gauge group $SU(2)$ on lattices of size $8^3 \times 4$, $16 \times 8^2 \times 4$ and $24 \times 12^2 \times 6$. The standard Wilson action

$$S_G(U) = \beta \sum_{n, \mu < \nu} \left[1 - \frac{1}{2} \text{Tr} (U_{n, \mu} U_{n+\mu, \nu} U_{n+\nu, \mu}^+ U_{n, \nu}^+) \right] \quad (2.10)$$

is used in our simulation. A combination of two algorithms, heatbath update and overrelaxation steps, has been employed for updating gauge fields. 40000 measurements for two smaller lattices and 20000 measurements for the largest lattice were done. We allowed 2000 sweeps for the thermalization of the gauge configurations. The deconfining transition point in the coupling constant values was identified through the location of the peak in the susceptibility of the Polyakov loop using Ferrenberg-Swendsen reweighting technique [6]. It was determined to be $\beta_c = 2.2985 \pm 0.0006$ for $N_{\tau} = 4$ and $\beta_c = 2.434 \pm 0.002$ for $N_{\tau} = 6$. In our algorithm four plaquettes are averaged in order to arrive at operator insertions that are symmetric in respect to a given lattice site n . It was found that the fluctuations are large in the quantity $L(0)L^+(\mathbf{r})\square$. A significant improvement is achieved by replacing $\langle \square_{\mu\nu} \rangle$ with $\square_{\mu\nu}(\mathbf{x}_R)$, where \mathbf{x}_R is the reference point placed far from the quark sources. This has no effect on the measured average value due to the cluster decomposition theorem [7], but the statistical errors are significantly reduced. Then Eq.(2.1) will be replaced with $f_{\mu\nu}(\mathbf{r}, \mathbf{x}) = \frac{\beta}{a^4} \left[\frac{\langle L(0)L^+(\mathbf{r})\square_{\mu\nu}(\mathbf{x}) \rangle - \langle L(0)L^+(\mathbf{r})\square_{\mu\nu}(\mathbf{x}_R) \rangle}{\langle L(0)L^+(\mathbf{r}) \rangle} \right]$. The signal in the correlations between a plaquette and Polyakov loops also tends to get drowned in the statistical noise when the distance between two Polyakov loops increases. Here we used a second

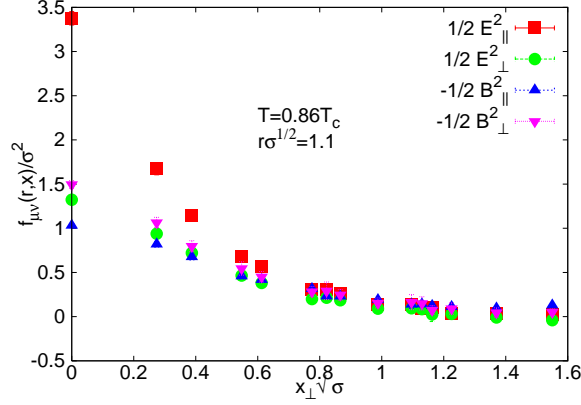


Figure 1: Comparison of electric and magnetic field components in the middle plane between two quark sources. Lattice size is $24 \times 12^2 \times 6$.

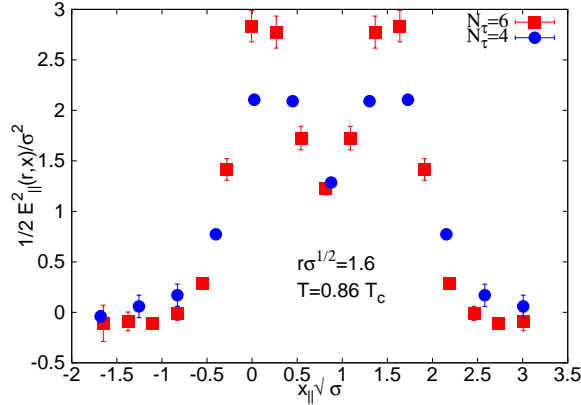


Figure 2: Longitudinal profile of $\frac{1}{2}E_{\parallel}^2$ at $x_{\perp} = 0$ for two values of N_{τ} .

noise reduction technique that is achieved by integrating out the temporal links in the Polyakov loops [8]. Our scaling function is based on the string tension results by [9]. We fit the data by the renormalization group inspired ansatz $\sqrt{\sigma}a(\beta) = R(\beta)(1 + c_2\hat{a}^2(\beta) + c_4\hat{a}^4(\beta))/c_0$ where $R(\beta) = (\frac{\beta}{2Nb_0})^{b_1/2b_0^2} \exp(-\frac{\beta}{4Nb_0})$ and $\hat{a}(\beta) = R(\beta)/R(\bar{\beta})$ with $\bar{\beta}$ chosen as $\bar{\beta} = 2.70$. The fit parameters we obtained as $c_0 = 0.00734 \pm 0.00006$, $c_2 = 0.06386 \pm 0.003$ and $c_4 = -0.003 \pm 0.0001$.

3. Results

Now we are in the position to show the results we have obtained. The comparison of electric and magnetic field components at given r and T is shown in Fig. 1. The parallel electric component is much larger than the other three components which are equal approximately. This holds for both below and above T_c . Furthermore, we observed finite a effects, which can be clearly seen from Fig. 2. Red square points correspond to the finer lattice spacing and are slightly smaller than the value corresponding at smaller N_{τ} value. The longitudinal and transverse distribution of $\frac{1}{2}E_{\parallel}^2$ as a function of T is given in Fig. 3. It has the peak values on the two sources on the left figure.

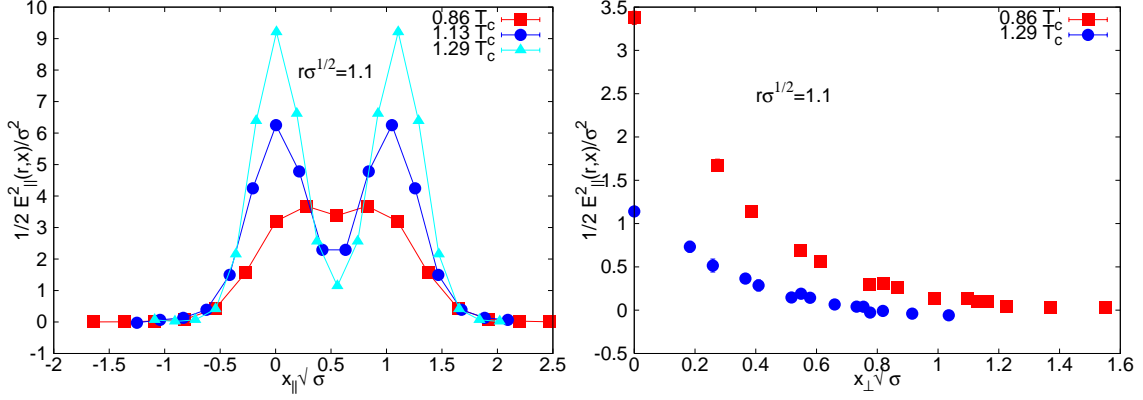


Figure 3: Left: Longitudinal profile of $\frac{1}{2}E_{\parallel}^2$ at $x_{\perp} = 0$; Right: Middle transverse profile at the same r .

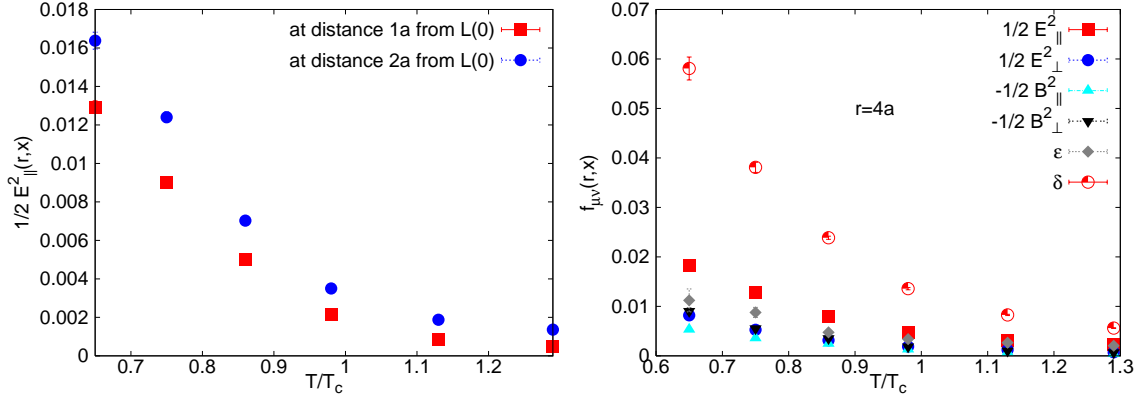


Figure 4: Left: Difference of values of $\frac{1}{2}E_{\parallel}^2$ distribution on inside and outside points of the flux tube as a function of T ; Right: Decrease of the middle point between the quark sources.

Along the longitudinal direction, away from the $q\bar{q}$ sources to outside the distribution decreases rapidly and it vanishes at distance about $x_{\parallel} = 0.5\text{fm}$. As one can see the distribution on the middle point between the sources decreases with T . Corresponding transverse profile is shown in the right figure, where one can also see the decrease of the half width of the tube with the T . It turned out that this also holds for larger separations. Moreover, this T -dependence is also true for $\frac{1}{2}B_{\parallel}^2$ except that the distribution value of $\frac{1}{2}B_{\parallel}^2$ is smaller than the $\frac{1}{2}E_{\parallel}^2$. Energy and action density are composed of total electric and magnetic fields, so the same features will also be seen for their T -dependence. The only difference is that the action density is much larger than the energy density because there is strong cancellation in the energy density term (see Eq. 2.8) due to the minus sign of the magnetic components, while the action density is amplified. One can watch the thinning of the flux tube with T by calculating the difference of values in inside and outside points of the tube. This is shown in the left plot of the Fig. 4, where there are two sets of data, one of which is difference of distribution values at $1a$ and $-1a$, away from a quark and the other one is the same at $2a$ and $-2a$. Each of them decreases with T and the two values at a given T are not only getting close to each other but also go to zero when T increases. This means that the field strength distribution approaches the one of a single isolated quark with rising temperature. The right plot of Fig. 4 shows the midpoint value

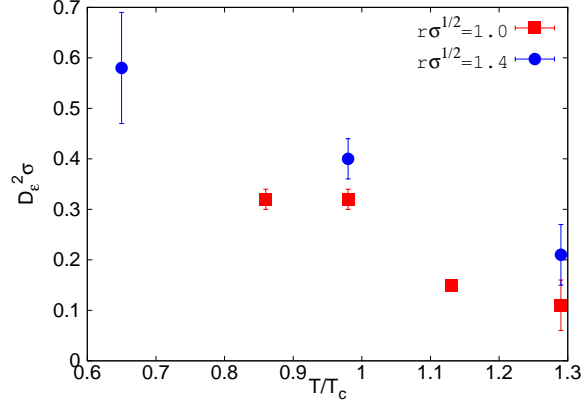


Figure 5: The mean squared width of the energy density, D_ε^2 , as a function of T , at two values of quark and an antiquark separation. The data are in units of the string tension and from a $24 \times 12^2 \times 6$ lattice.

between sources for each observable as a function of T . The action density is the largest one and secondly parallel electric and so on. They all decrease with T to zero, which means height of the flux tube decreases with T . We have already seen from the transverse profiles that the half width of the distribution decreases with T . In order to estimate it quantitatively we fit the transverse profiles of the field strengths on the center plane between $q\bar{q}$ pair, for various β values. The fitted form [2] is

$$\frac{1}{2\beta} E_\perp^2(r, x_\perp) = -\frac{1}{2\beta} B_\parallel^2(r, x_\perp) = -\frac{1}{2\beta} B_\perp^2(r, x_\perp) = a_1 e^{-a_2 x_\perp}, \quad (3.1)$$

$$\frac{1}{2\beta} E_\parallel^2(r, x_\perp) = \frac{a_1}{(a_2 + x_\perp^2)^3} + a_1^{(\varepsilon)} e^{-a_2^{(\varepsilon)} x_\perp} \quad (3.2)$$

From the resulting fit parameters we determine the width of the flux tube defined via [2]

$$D_{\varepsilon, \delta}/a = \sqrt{\frac{\int d^2 x_\perp x_\perp^2 (E^2 \pm B^2)}{\int d^2 x_\perp (E^2 \pm B^2)}}. \quad (3.3)$$

The width of the energy and action density, corresponding to the $+/-$ sign, are denoted by an index ε and δ respectively. The width of the energy density is given by $a^{-2} D_\varepsilon^2 = \frac{6}{(a_2^{(\varepsilon)})^2}$. Here we show only the width of the energy density in Fig. 5. We call the width of the energy density the physical width of the flux tube. At $r\sqrt{\sigma} = 1.0$, the mean squared width of the energy density, D_ε^2 , decreases as T increases. The same dependence on T holds for larger separations, namely at $r\sqrt{\sigma} = 1.4$.

4. Conclusions

We have studied field distributions around a static $q\bar{q}$ pair at finite T using Polyakov loop plaquette correlations at physical quark separations up to 1.4fm. T range was $0.7 - 1.3T_c$. Measuring the electric and magnetic components of the field in close vicinity of the phase transition using Monte Carlo numerical simulation, we were able to see various (i.e longitudinal and transverse)

profiles of the flux tube. From the profiles at various T we find that the physical width of the flux tube decreases when T increases. The fall of the width and height with T at the same time shows the gradual disappearance of the flux tube when the temperature approaches T_c .

References

- [1] O. Kaczmarek, F. Karsch, E. Laermann and M. Lütgemeier, *Heavy quark potentials in quenched QCD at high temperature*, *Phys. Rev. D* **62** (2000) 034021.
- [2] R. Sommer, *Scaling of $SU(2)$ flux distribution and potential*, *Nucl. Phys.* **B291** (1988) 673.
- [3] R. W. Haymaker and J. Wosiek, *Distribution of the color fields around static quarks: Lattice sum rules*, *Phys. Rev. D* **43** (1991) 2676.
- [4] G. S. Bali, K. Schilling and Ch. Schlichter, *Observing long color flux Tubes in $SU(2)$ lattice gauge theory*, *Phys. Rev. D* **51** (1995) 5165 [hep-lat/9409005].
- [5] R. W. Haymaker, V. Singh and Y. Peng, *Distribution of the color fields around static quarks: Flux tube profiles*, *Phys. Rev. D* **53** (1996) 389 [hep-lat/9406021].
- [6] Alan M. Ferrenberg and Robert H. Swendsen, *New Monte Carlo technique for studying phase transitions*, *Phys. Rev. Lett.* **61** (1988) 2635.
- [7] R. W. Haymaker and Y. Peng, *$SU(2)$ flux distributions on finite lattices*, *Phys. Rev. D* **47** (1993) 5104.
- [8] G. Parisi, R. Petronzio and F. Rapuano, *A Measurement of the string tension near the continuum limit*, *Phys. Lett.* **B128** (1983) 418.
- [9] J. Engels, J. Fingberg and D. Miller, *Phenomenological renormalization and scaling behaviour of $SU(2)$ lattice gauge theory*, *Nucl. Phys.* **B387** (1992) 501.